RESEARCH PAPER

BURNED AREA DETECTION USING CONVOLUTIONAL NEURAL NETWORK BASED ON SPATIAL INFORMATION OF SYNTHETIC APERTURE RADAR DATA IN INDONESIA

Anugrah Indah Lestari[1*], Dony Kushardono[1], Athar Abdurrahman Bayanuddin[2]
[1]National Research and Innovation Agency, Cibinong, West Java, Indonesia 16911
[2]Directorate of Laboratory Management, Research Facilities, and Science and Technology Park, National Research and Innovation Agency, Parepare, South Sulawesi, Indonesia 91131
***Corresponding author:** anugrah.indah.lestari@brin.go.id
Received: November 2nd 2023 / Accepted: April 10th 2024 / Published: July 1st 2024
https://DOI-10.24057/2071-9388-2024-3109

ABSTRACT. Forest and land fires are disasters that often occur in Indonesia which affects neighbouring countries. The burned area can be observed using remote sensing. Synthetic aperture radar (SAR) sensor data is advantageous since it can penetrate clouds and smoke. However, image analysis of SAR data differs from optical data, which is based on properties such as intensity, texture, and polarimetric feature. This research aims to propose a method to detect burned areas from the extracted feature of Sentinel-1 data. The features were classified using the Convolutional Neural Network (CNN) classifier. To find the best input features, several classification schemes were tested, including intensity and polarimetric features by applying the Boxcar speckle filter and the Gray Level Co-occurrence Matrix (GLCM) texture feature without using the Boxcar speckle filter. Additionally, this research investigates the significance of a window size parameter for each scheme. The results show the highest overall accuracy achieved 84% using CNN classification utilizing the GLCM texture features and without conducting the Boxcar speckle filter on the window size of 17×17 pixels when tested on the part region of Pulang Pisau Regency and Kapuas Regency, Central Kalimantan in 2019. The total burned area was 76,098.6 ha. The use of GLCM texture features without conducting the Boxcar speckle filter as input classification performs better than using intensity and polarimetric features that undergo the Boxcar speckle filter. Combining intensity and polarimetric features with performing the Boxcar speckle filter improves better classification performance over utilizing them separately. Furthermore, the selection of window size also contributes to improve the model performance.

KEYWORDS: burned area, convolutional neural network, gray level co-occurrence matrix texture feature, synthetic aperture radar

CITATION: Lestari A. I., Kushardono D., Bayanuddin A. A. (2024). Burned Area Detection Using Convolutional Neural Network Based On Spatial Information Of Synthetic Aperture Radar Data In Indonesia. Geography, Environment, Sustainability, 2(17), 36-48
https://DOI-10.24057/2071-9388-2024-3109

ACKNOWLEDGEMENTS: The authors sincerely thank the Research Center for Remote Sensing, Research Organization for Aeronautics and Space, National Research and Innovation Agency for providing very-high resolution images. Also, the authors would like to acknowledge the Ministry of Environment and Forestry Republic of Indonesia for providing Burned Area and Land Cover Maps.

Conflict of interests: The authors reported no potential conflict of interest.

INTRODUCTION

The land and forest fires that occurred in Indonesia become an international issue since they affect bordering countries. Land and forest fire incidents cause several environmental and health issues due to air pollution from the fog, bad haze, and carbon in the air (Ho et al. 2019). In 2019, Malaysia and Singapore endured the suffocating presence of a thick haze for an entire week, causing severe air pollution and discomfort in both countries, due to transboundary haze from Indonesia (Nguyen et al. 2022; Sakti et al. 2023; Yeung 2019[1]). According to the report of the Ministry of Environment and Forestry (MoEF) Republic of Indonesia[2], the most severe burned occurrence in Indonesia happened in 2015 up to 2.6 million hectares, followed by 1.64 million hectares in 2019, primarily in Kalimantan and Sumatera Islands (Ministry of Environment and Forestry 2019).

[1]Yeung, J. (2019) Indonesian forests are burning, and Malaysia and Singapore are choking on the fumes. [online] Available at: https://www.huahintoday.com/sports/indonesian-forests-still-burning-and-malaysia-and-singapore-are-choking-on-the-fumes/#:~:text=More%20than%20930%2C000%20hectares%20%28about%202.3%20million%20acres%29,all%20week%2C%20with%20air%20quality%20reaching%20unhealthy%20levels [Accessed 20 June 2023]
[2] Ministry of Environment and Forestry (MoEF) Republic of Indonesia. (2019). Recapitulation of Forest and Land Fire Area (Ha) per Province in Indonesia. (in Indonesian). [online] Available at: https://sipongi.menlhk.go.id/ [Accessed 21 Apr 2023]

The Indonesian government has been implementing some strategies for land and forest fire management since 2015. One of the strategies is a method development for calculating the burned areas. Monitoring the fire event requires the use of remote sensing data for burned area mapping as part of a system from detection to post-fire management (Efransjah et al. 2020). Some optical imageries such as Landsat and Sentinel-2 have been utilized as the primary data for mapping the burned area as the main data. Recently, the automatic mapping approach has been developed by the Indonesian government, but it is still in the early stages of development (Efransjah et al. 2022). However, the presence of clouds or smoke above the burned areas limits the observation utilizing the optical remote sensing data. The use of multi-sensor satellite imageries is a solution to generate a better-burned area map by combining optical and SAR satellite imageries (Abdikan et al. 2022; Arjasakusuma et al. 2022; Sudiana et al. 2023). Single satellite data input can lead to underestimating burned area calculations due to fewer revisit times. Gaveau et al report that using Setinel-2 data resulted in the burned area in 2019 reaching 3.11 Mha across Indonesia (Gaveau et al. 2021). It was twice as estimated by the Indonesian government's MOEF by using manual delineation on Landsat-8 images. On the other hand, stand-alone SAR data has the ability to generate high accuracy in burned area mapping.

Synthetic aperture radar (SAR) is a non-optical sensor of remote sensing that has been investigated for use in burned area mapping (Ban et al. 2020; Hosseini and Lim 2023; Tanase et al. 2010), mainly because it can penetrate the cloud and the smoke over the burned areas, non-weather depends as well. Some studies have been investigating Sentinel-1's capability to map the burned areas, using interferometric coherence and backscatter time series (Tanase et al. 2020), unsupervised classification using radar properties (De Luca et al. 2021), random forest (Hosseini and Lim 2023), deep learning CNN (Luft et al. 2022), and near real-time monitoring using a deep learning approach (Ban et al. 2020), as well as the automatic framework using Deep Convolutional Neural Network (DCNN) (Radman et al. 2023).

Texture features and polarimetric features are important extracted features that need to be selected in classification using SAR images (Singh and Kaur 2011). An urban land cover classification was studied using an SAR image. It results in selected texture features such as mean intensity, semivariograms, variance, and weighted-rank fill ratio improving the classification result (Dekker 2003). SAR image classification using the Sandia National Laboratories dataset was performed using texture features such as gray level co-occurrence matrix (GLCM) and Gabor filters (GFs) and reduced using canonical correlation analysis (CCA). It results in good performance and high efficiency (Ismail et al. 2014). The Sentinel-1 image's texture features were used to identify lead using a random forest algorithm, which resulted in high precision (Murashkin et al. 2018). Furthermore, window size is an important parameter in texture features as a larger window size tends to give stable results (Wen et al. 2009).

Besides the texture features and polarimetric features, speckle is a type of noise that may influence the results of the application obtained from the SAR data. A comparison among several despeckling methods was performed such as Frost, Gamma maximum a posteriori (MAP), Lee, Median, and Boxcar filter using Sentinel-1 images, resulting in the Boxcar filter outperforming them in identifying mangrove forests (Ansari et al. 2020). Also, the boxcar filter proved easy and effective for homogenous regions (Mullissa et al. 2022).

In the matter of Indonesia's burned area mapping, the research regarding the optimum feature of Sentinel-1 C-band SAR is still insufficient. Moreover, adequate radar input features are needed since Indonesia consists of various landscapes to obtain high accuracy in burned area detection. Therefore, this research proposed a method to detect burned areas based on our investigation from the extracted feature of Sentinel-1 data. The extracted feature is then classified using the 1-D CNN classifier since CNN can be treated as state-of-the-art in image classification. We investigate several classification schemes from the extracted features of σ^0 and γ^0 in VH and VV polarization of mosaic images in pre-fire events as well as post-fire events such as intensity and polarimetric features with performing Boxcar speckle filtering as well as GLCM texture feature without performing Boxcar speckle filter to look for the optimum parameter.

MATERIALS AND METHODS

Research Location and Data

This research examined a subset of Pulang Pisau Regency and Kapuas Regency, Central Kalimantan, Indonesia (see Fig. 1) since this province is one of the most affected regions in 2019 (MoEF 2019). Generally, the Muller and Swachner and hilly areas dominate the northern part of this province, while the lowland zone, swamp, and brackish lie in the southern part (Central Kalimantan Province Environmental Agency 2020). The ecosystems found in Central Kalimantan are rain forest, peat forest, heath forest, swamp forest, lowland forest, upland forest, mangrove forests, and plantation forest (Center for Kalimantan Ecoregion Development Control Ministry of Environment and Forestry 2016; Central Kalimantan Province Environmental Agency 2020). According to Statistics Indonesia, Pulang Pisau Regency and Kapuas Regency have various land cover types including hilly areas in the north region and swamps as well as coastal areas in the south area (Statistics Indonesia 2010, 2023). According to the Land Cover Map from the MoEF, the research area's land cover types include swamp, shrub swamp, shrub, bare land, plantation, built-up land, mangrove, secondary swamp forest, paddy field, and agriculture area, as illustrated in Fig. 1.

This research used Sentinel-1 GRD data derived from Google Earth Engine. Table 1 provides detailed information about the Sentinel-1 data used in this research. The date description in Table 1 indicates that pre-fire events occurred from 6-23 July 2019, while post-fire events occurred from 10-27 October 2019. As the classification was a supervised approach, Fig. 2 shows the Satellite pour de l'Observation de la Terre (SPOT) images dated 2 September and 8 October 2019, as well as 10 October 2018 with a resolution of 1.5 meters that were used in this research as the reference data. The Land Cover Map from the MoEF in 2019, was utilized to determine the land cover type at the research site. The active fire data from MODIS and the Visible Infrared Imaging Radiometer Suite (VIIRS) sensor in July – October 2019, collected from the National Aeronautics and Space Administration (NASA), were used in this research as a consideration of the occurrence of burned areas. Furthermore, MODIS's burned area monthly global 500 m, MCD64A1, derived from Google Earth Engine, was employed in this research. The burned area information from the MoEF in 2019 was also used to find out the burned area location and month of fire.

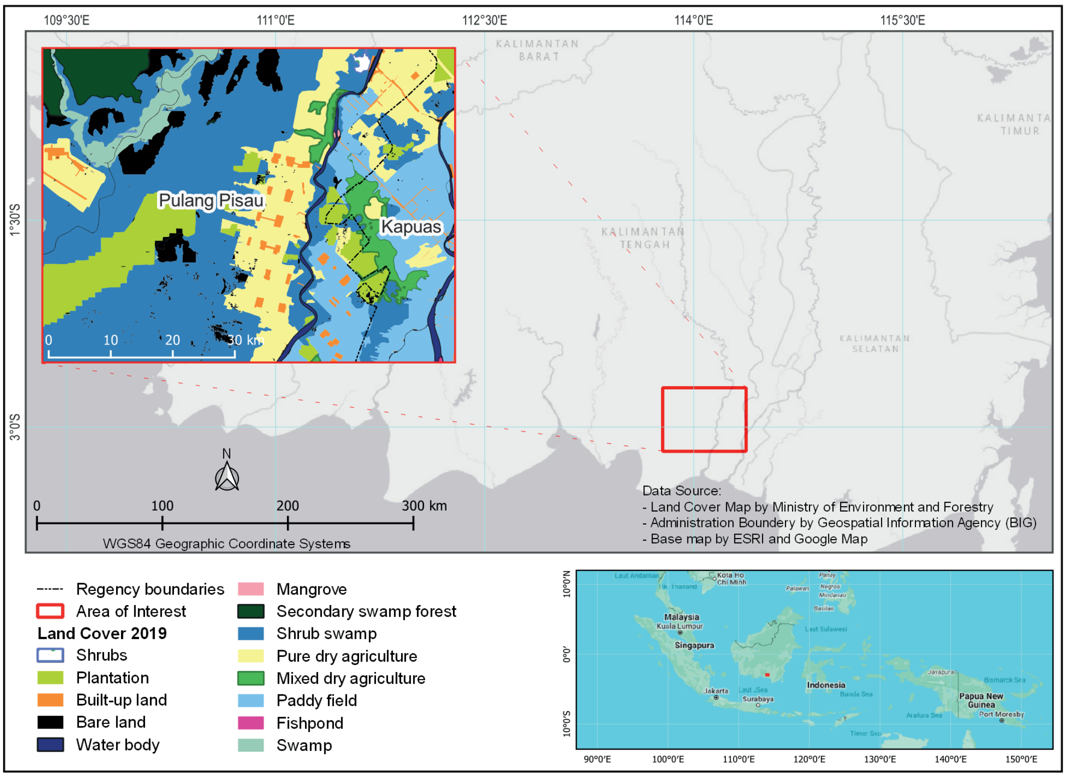

Fig. 1. The area of interest (red rectangle) investigated in the research

Table 1. Sentinel-1 data details for the research

Parameters	Descriptions	
Date	Pre-fire: July 2019	Post-fire: October 2019
Frequency	5.405 GHz	
Pixel Spacing	10 meters	
Orbit	Descending	
Product Type	Ground range detected (GRD)	
Acquisition Mode	Interferometric wide swath	
Polarization Mode	VV and VH	

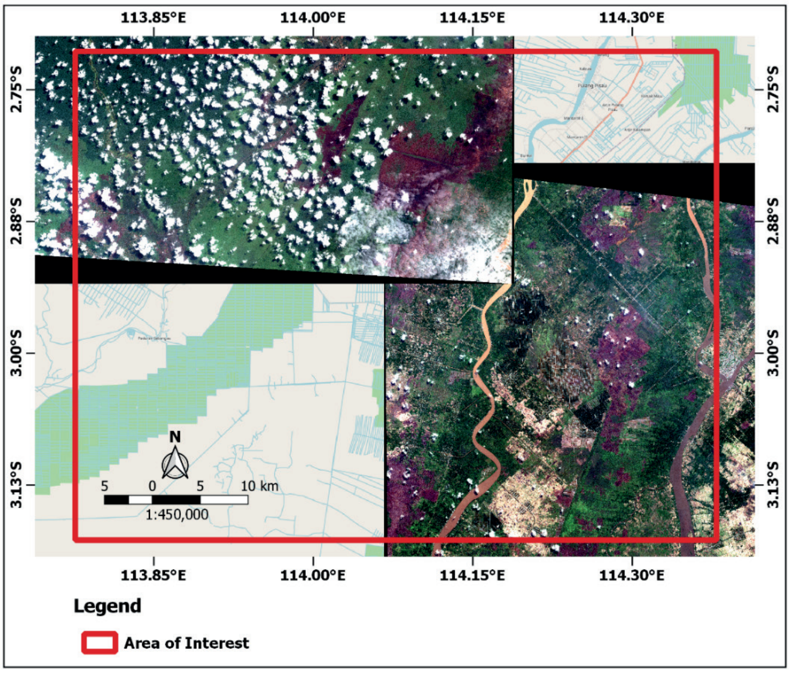

Fig. 2. SPOT data coverage in an area of interest

Methodology

Fig. 3 depicts the flowchart used in this study. It comprises image pre-processing, training and validation data construction, classification, performance evaluation, and burned area information generation.

The SAR data pre-processing was performed using Google Earth Engine (GEE) which includes producing gamma nought (γ^0) from sigma nought (σ^0). This research utilized two types of two backscatter coefficients namely σ^0 and γ^0 on VH and VV polarizations. σ^0 is described as an average of radar reflectivity per unit area in the ground plane (Hossain and Easson 2009; Small 2011), while γ^0 is the reflected radar signal per unit area perpendicular to the slant plane (Small 2011). As σ^0 relies on a variance of the incidence angle, γ0 can assist in minimizing incidence angle dependence (Emery and Camps 2017). These backscatter coefficients can be expressed in mathematical expression as follows (Srivastava et al. 2022):

$$\sigma^0 = 10\log_{10}(DN^2) + K \quad (1)$$

$$\gamma^0 = \frac{\sigma^0}{\cos\theta} \quad (2)$$

where DN is digital number from SAR amplitude image, K is a calibration factor, and θ is incidence angle.

After the pre-processing step, feature extraction and Gray Level Co-occurrence Matrix (GLCM) texture feature extraction were performed. Before feature extraction, the investigation was performed by implementing the Boxcar speckle. The Boxcar filter is basically an averaging filter that changes the centre pixel by a mean value of a moving window N × N (Yahia et al. 2020). Meanwhile, the GLCM texture feature was extracted without speckle filtering, as shown in Fig. 3. The variation of window size was conducted in speckle filtering and GLCM texture feature extraction, with the following pixel sizes 5×5, 7×7, 9×9, 11×11, 13×13, 15×15, and 17×17. This disparate experiment was done to understand the effectiveness of feature extraction after the Boxcar speckle filter, compared with the performance of GLCM texture feature extraction with differing window sizes.

The selection of training and validation data was performed by interpreting SPOT data as a reference, which is shown in Fig. 2. The model was developed using Convolutional Neural Network 1D (CNN-1D). Following that, classification was performed to obtain the burned area information.

Polarimetric and Texture Features

This research used several features such as radar burn ratio (RBR), radar burn difference (RBD), Δ radar vegetation index (ΔRVI), and Δ dual-polarization SAR vegetation index (ΔDPSVI). RBR and RBD on VH polarization perform well in differentiating between burned and unburned areas (Lasaponara and Tucci 2019). In addition, RVI and DPSVI are good indicators of backscatter changes mainly for vegetation (De Luca et al. 2021; Mandal et al. 2020; Periasamy 2018). These features can be expressed as follows:

$$RBR_{xy} = \log_{10}\frac{Post-fire\ average\ backscatter_{xy}}{Pre-fire\ average\ backscatter_{xy}} \quad (3)$$

$$RBD_{xy} = Post\text{-}fire\ average\ backscatter_{xy} - \\ - Pre\text{-}fire\ average\ backscatter_{xy} \quad (4)$$

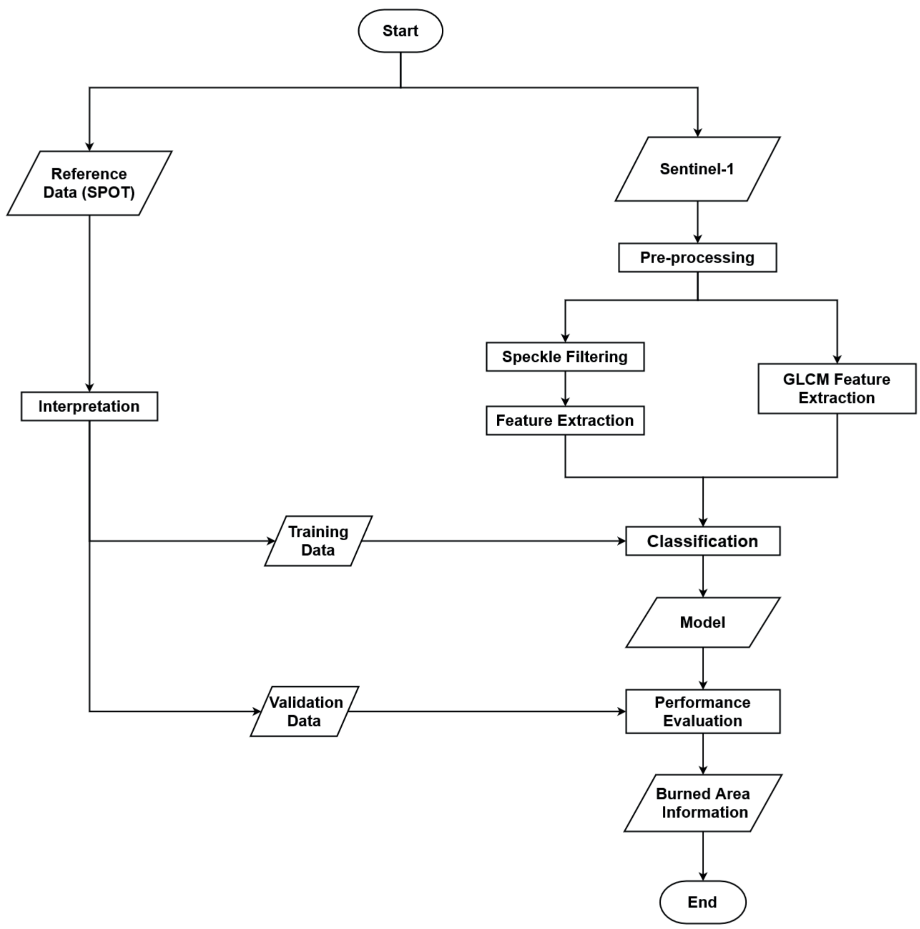

Fig. 3. Research flowchart

$$RVI = \frac{4VH_{time\ average}}{VV_{time\ average} + VH_{time\ average}} \quad (5)$$

$$DPSVI = \frac{VV_{time\ average} + VH_{time\ average}}{VV_{time\ average}} \quad (6)$$

GLCM is an important texture feature that has been used in SAR image processing for several applications (Champion et al. 2014; James et al. 2021; Lestari et al. 2021; Soh and Tsatsoulis 1999). This research used several GLCM texture features such as contrast, entropy, homogeneity, and mean since the features are adequate to discriminate between burned and unburned areas (Mutai 2019). Table 2 shows the mathematical expression of the used GLCM texture features (Anand et al. 2023).

Training and Validation Dataset Generation

In constructing the dataset, high-resolution SPOT images were utilized to label burned and unburned areas. Besides, the occurrence of burned areas was also checked using high-level confidence in burned area information from the MoEF, which means the area had been checked by field investigation. The dataset was divided into training and validation data, which comprised burned and unburned classes. The distribution between the training and validation datasets was 70:30. This research collected 176,100 pixels, which contained 88,460 pixels of burned and 87,640 of unburned classes for training, and 76,032 pixels comprising 38,632 of burned and 37,400 of unburned classes for validation.

Classification Schematic

To examine the optimum classification parameter for burned area detection, there are four schemes that were investigated in this research as shown in Table 3. In the first scheme, σ^0 and γ^0 of mosaic images in pre-fire events and post-fire events were used as inputs, resulting in 8 bands. Then, indices logRBR, RBD, ΔRVI, ΔDPSVI on σ^0 and γ^0 were utilized for Scheme -2, so the inputs become 12 bands. Next, the inputs on Scheme -1 and Scheme -2 were combined and were investigated in Scheme -3. Last, GLCM texture features were used as inputs for Schemes -4.

Classification Design

A convolutional neural network (CNN) is a deep learning type that has the advantage of being able to extract features automatically (LeCun et al. 2015). This research focuses on 1-D CNN where the architecture is built and trained using one-dimensional data. 1-D CNN has the advantage of having relatively low computational complexity and computational requirements so that it can be used for real-time applications (Kiranyaz et al. 2021). In addition, for the utilization of remote sensing data, the use of multi-temporal remote sensing data and the CNN 1-D method is effective in increasing the accuracy of up to 1.9% (Guidici and Clark 2017) and 4% (Song et al. 2019) in classifying land cover. Generally, CNN is a network consisting of several layers where the previous layer's output is connected in sequential order to the next input involving trained weights and biases. CNN comprises three main operations: convolution, nonlinearity, and pooling/subsampling (Zhang et al. 2018). An architecture of one-dimensional CNN consists of an input layer, a convolutional layer, a pooling layer, and a fully connected layer. This research used two convolutional layers, one pooling layer, one dropout layer, and two hidden layers. In this research, the convolutional layers used a kernel size of 2 × 2. The hidden layer used a Rectified Linear Unit as an activation function. A sigmoid function was utilized in the output layer. In addition, the Adam optimizer and binary cross-entropy were utilized as they classify two classes. The learning rate was set to 0.001 with an epoch of 500.

Table 2. Mathematical expression of the GLCM texture features used in the research

GLCM Texture Feature	Mathematical Expression
Contrast	$\sum_{n=1}^{L} n^2 \sum_{x=1}^{L} \sum_{X=1}^{L} P(x,y)$
Entropy	$-\sum_{x=1}^{L} \sum_{X=1}^{L} P(x,y)\, lgP(x,y)$
Homogeneity	$\sum_{x=1}^{L} \sum_{X=1}^{L} \lvert i-j \rvert P(x,y)$
Mean	$\sum_{x=1}^{L} \sum_{X=1}^{L} x.P(x,y)$

Table 3. Classification schemes

Scheme	Bands/Features
1	8 bands VH and VV polarization of σ^0 and γ^0 of pre-fire and post-fire events
2	12 bands of logRBR, RBD, ΔRVI, ΔDPSVI on σ^0 and γ^0
3	20 bands with features consist of Scheme -1 and Scheme -2
4	32 texture feature bands VH and VV polarization of σ^0 and $\gamma^0$of homogeneity, entropy, contrast, and mean in pre-fire and post-fire events

The classification model development was conducted using a workstation with the specifications of an Intel Xeon Gold 6130 CPU @2.10 GHz, and 32 GB RAM. In addition, the Python programming language was used for a deep learning model development using the "TensorFlow" and "Keras" libraries. Geospatial Data Abstraction Library (GDAL) was employed for supervising geospatial image processing, such as data type conversion.

Performance Metrics

Several metrics were used to evaluate the classification model's performance, i.e., overall accuracy (OA), precision, recall, F1-Score, and Cohen's Kappa (K) as stated in Eq. (7) – (11). Overall accuracy is the ratio between our model correctly classified and all the tested data namely true positive (TP), true negative (TN), false positive (FP), and false negative (FN). Precision shows a portion of the predicted burned class that is correct. The recall implies the proportion of a class that is classified correctly based on reference data information (ground truth). Precision and recall become the optimum parameters for class imbalance problems. Meanwhile, the F1-Score is the metric that combines precision and recall and utilizes their harmonic mean. Cohen's Kappa is used to measure the degree of agreement between the predicted results and the reference data. The pe value in Equation (11) shows the probability of change between the predicted results and the reference data (Molin and Jee 2021).

$$Overall\ accuracy\ (OA) = \frac{TP+TN}{TP+TN+FP+FN} \tag{7}$$

$$Precision = \frac{TP}{TP+FP} \tag{8}$$

$$Recall = \frac{TP}{TP+FP} \tag{9}$$

$$F1-Score = 2\times\frac{(Precision \times Recall)}{(Precision \times Recall)} \tag{10}$$

$$Cohen's\ Kappa\ (K) = \frac{Overall\ accuracy - \rho_e}{1-\rho_e} \tag{11}$$

RESULTS

Burned Area Detection Classification Result for Every Scheme

In Scheme -1, where the 8 bands SAR data undergo Boxcar filter, the highest OA, F1-Score, and K values were found in the window size of 13×13 are 0.8060; 0.8050; and 0.6121 respectively as shown in Table 4. For precision and recall values, window sizes of 15×15 and 11×11 were found to be the best settings for precision and recall scores in both performance evaluations. As stated in (Landis and Koff, 1977), this finding demonstrates that the K value using window sizes of 13×13 and 17×17 was categorized as a substantial agreement for Scheme -1, while the other window sizes were categorized as moderate agreement.

Scheme -2 used 12 bands of SAR features that undergo Boxcar filtering as inputs. The window size of 15×15 yielded the highest OA and K values of 0.7822 and 0.5648, respectively. For precision, recall, and F1-score values, the highest value was achieved at a window size of 13×13, 9×9, and 11×11 respectively. The model in Scheme -2 with various window sizes shows an agreement between predicted results and reference data that was categorized as moderate agreement (ranging from 0.4570-0.5648) as shown in Table 4.

In Scheme -3, in which the inputs were a combination of Scheme -1 and Scheme -2 SAR features, the highest OA, recall, F1-Score, and K values were found at a window size of 17×17 with the following value namely 0.8342; 0.8204; 0.8341; and 0.6685 respectively. For precision value, window sizes of 13×13 was the most effective parameter for obtaining the highest value. In Scheme -3, the model showed substantial agreement, except when using a window size of 5×5 based on K value.

In Scheme -4, in which the inputs were the selected GLCM texture features, a window size of 17×17 resulted in the highest OA, recall, precision, F1-Score, and K with the following value of 0.8461; 0.8035; 0.8831; 0.8414; and 0.6926 respectively. In this scheme, a substantial agreement was found in the model with a window size of 13×13, 15×15, and 17×17, while the others were moderate agreement as seen in Table 3.

These results also indicate that an increase in the number of features for classification will result in a longer processing time during training, as demonstrated by Scheme -4, which utilizes the most features. However, increasing the window size does not necessarily increase the training time as depicted in Schemes -1- 4 in Table 4.

Performance Comparison of Different Schemes in Detecting Burned Areas

Fig. 4 depicts the comparison of burned area classification performance indicated by OA, recall, precision, F1-score, and K in each scheme. Comparing Scheme -1 to -4, the highest OA, precision, F1-Score, and K values were achieved in the model Scheme -4 with a window size of 17×17, as shown in Fig. 4. It means that this model has a potency to minimize a mistake in determining the burned area which should be an unburned area. Fig. 5 shows the burned area classification result using Scheme -4 with a window size of 17×17. The highest recall value was in Scheme -3 with a window size of 17×17. This finding also indicates that the burned areas in the area of interest are primarily found in shrub swamps, pure dry agriculture, and paddy fields. It reveals that the burned areas occurred caused by anthropogenic activities.

Compared to Scheme -1 and Scheme -2, combined SAR features such as intensity and polarimetric features in Scheme -3 help to boost the performance in each window size. Additionally, the findings emphasize the importance of selecting SAR features with different window sizes to improve the model's classification performance This research also demonstrates the feasibility of using combined SAR features in Schemes -1 and -2, along with Boxcar's speckle filter in Scheme -3, and Scheme -4, which employs the GLCM texture feature without speckle filtering, for burned area detection.

Fig. 6 displays the results of burned area detection on a selected area in Scheme-1 which has window size of 5×5, and Scheme-4 which has window size of 17×17, representing the worst and the best models, respectively. The blue polygon in Fig. 6 represents a burned area reference derived from SPOT images. When comparing the two figures visually, misclassification of the burned area is mostly on a window size of 5×5 which shows the inability to show burned area patterns as indicated by the yellow and

Table 4. The performance results of burned area classification using the CNN methods for Schemes -1 to -4

Window Size	Scheme -1					
	OA	Recall	Precision	F1 -Score	K	Training Time (min)
5×5	0.7194	0.6903	0.7400	0.7142	0.4392	208.48
7×7	0.7474	0.7429	0.7558	0.7493	0.4949	204.51
9×9	0.7768	0.7772	0.7821	0.7796	0.5535	202.77
11×11	0.7941	0.8116	0.7892	0.8003	0.5880	195.45
13×13	0.8060	0.7882	0.8225	0.8050	0.6121	199.44
15×15	0.7987	0.7553	0.8330	0.7923	0.5980	201.06
17×17	0.8029	0.7950	0.8130	0.8039	0.6059	199.67
Window Size	Scheme -2					
5×5	0.7285	0.7308	0.7338	0.7323	0.4570	234.38
7×7	0.7513	0.7714	0.7473	0.7592	0.5023	229.19
9×9	0.7747	0.7903	0.7718	0.7809	0.5492	229.12
11×11	0.7799	0.7727	0.7897	0.7811	0.5599	227.51
13×13	0.7777	0.7307	0.8128	0.7696	0.5559	221.47
15×15	0.7822	0.7491	0.8082	0.7775	0.5648	225.03
17×17	0.7752	0.7402	0.8020	0.7699	0.5508	231.16
Window Size	Scheme -3					
5×5	0.7635	0.7834	0.7588	0.7709	0.5265	264.69
7×7	0.8024	0.7943	0.8126	0.8033	0.6048	271.84
9×9	0.8026	0.7909	0.8151	0.8028	0.6052	274.34
11×11	0.8130	0.7709	0.8473	0.8073	0.6265	263.05
13×13	0.8183	0.7810	0.8493	0.8137	0.6370	263.91
15×15	0.8226	0.8176	0.8307	0.8241	0.6453	273.81
17×17	0.8342	0.8204	0.8483	0.8341	0.6685	270.40
Window Size	Scheme -4					
5×5	0.7043	0.7686	0.6868	0.7254	0.4074	323.22
7×7	0.7410	0.7125	0.7622	0.7365	0.4824	326.04
9×9	0.7760	0.7997	0.7687	0.7839	0.5515	317.50
11×11	0.7931	0.7480	0.8282	0.7861	0.5868	330.08
13×13	0.8204	0.7869	0.8486	0.8166	0.6411	319.72
15×15	0.8252	0.7944	0.8516	0.8220	0.6507	326.07
17×17	0.8461	0.8035	0.8831	0.8414	0.6926	330.66

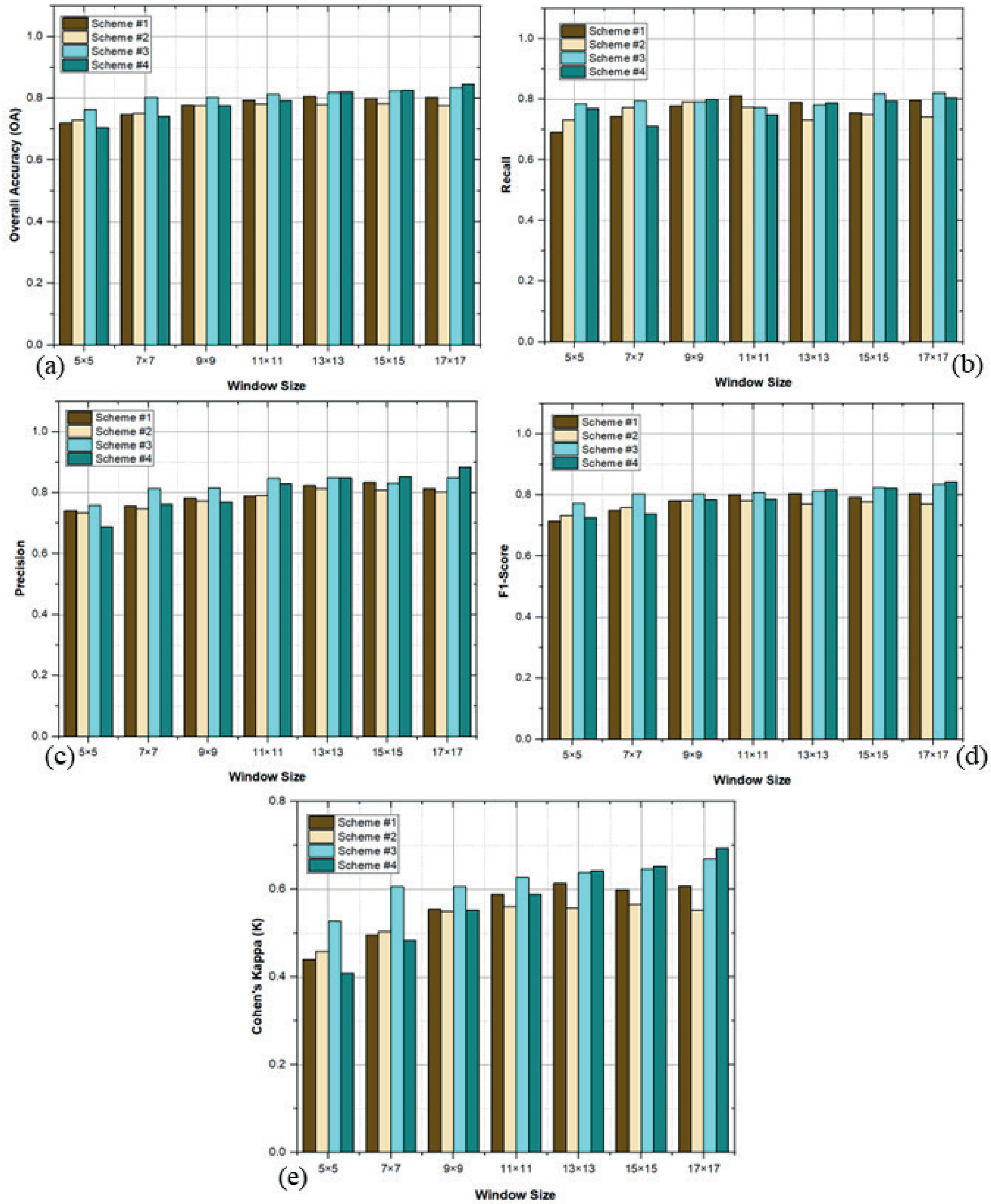

Fig. 4. Performance of burned area classification model using CNN method for Scheme -1 to -4 with performance metrics (a) OA; (b) recall; (c) precision; (d) F1-score; (e) Cohen's Kappa

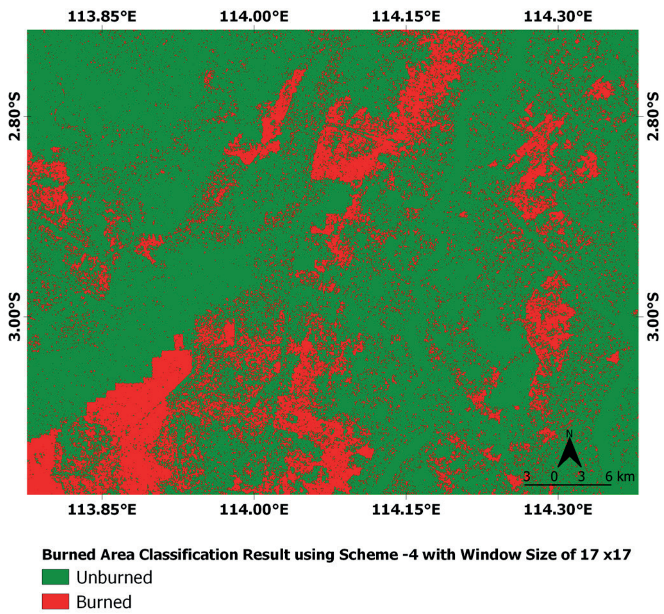

Fig. 5. Burned area classification result for Scheme -4 with a window size of 17×17

orange colours from the Sentinel-1 in Fig 6a. Furthermore, several pixels on the outside of the blue polygon, which are shrub and agricultural area, are incorrectly identified as burned areas. This may occur because the speckle filter's window size is insufficient for extracting surface roughness information between objects. Consequently, finding the optimal window size is essential in acquiring object information, and increasing the window size may reduce misclassification.

Burned Area Estimation

The total burned area in our area of interest based on the best performance is 76,098.6 ha. It includes the total of burned area that is not covered by the SPOT imageries as shown in Fig. 2. It also demonstrates that the Sentinel-1 is successful in identifying the burned area even it is covered by the cloud. Fig. 7 depicts the comparison of the selected subset of burned area classification results between the Scheme -1 with the lowest performance (window size of 5×5) and the Scheme -4 with the highest performance (window size of 17×17), as well as SPOT image is used as reference visually. It shows a misclassification mainly occurred in Scheme -1 with the window size of 5×5 (see Fig 7b). It fails to accentuate the pattern of burned areas and there is no clear boundary between burned and unburned classes. It is proven by the low value of recall. There are a lot of small pixels identified as burn areas which spread almost all the subset, except for the water body that was almost completely identified as unburned areas.

As shown in Fig. 7c, compared to the Figs. 7a and 7b, the burned areas were shaped in a better pattern and were more compact (see white circle on the right). The little pixels identified as unburned areas inside the burned land area had been minimized and aggregated into bigger polygons for the misclassification of unburned areas outside the burned land. However, it still left several areas spread outside the burned land that were misclassified as burned areas. The misclassification of the burned area from Figs. 7b and 7c is shown by the bare land area for plantations that is indicated as devegetation (see yellow circle on the left).

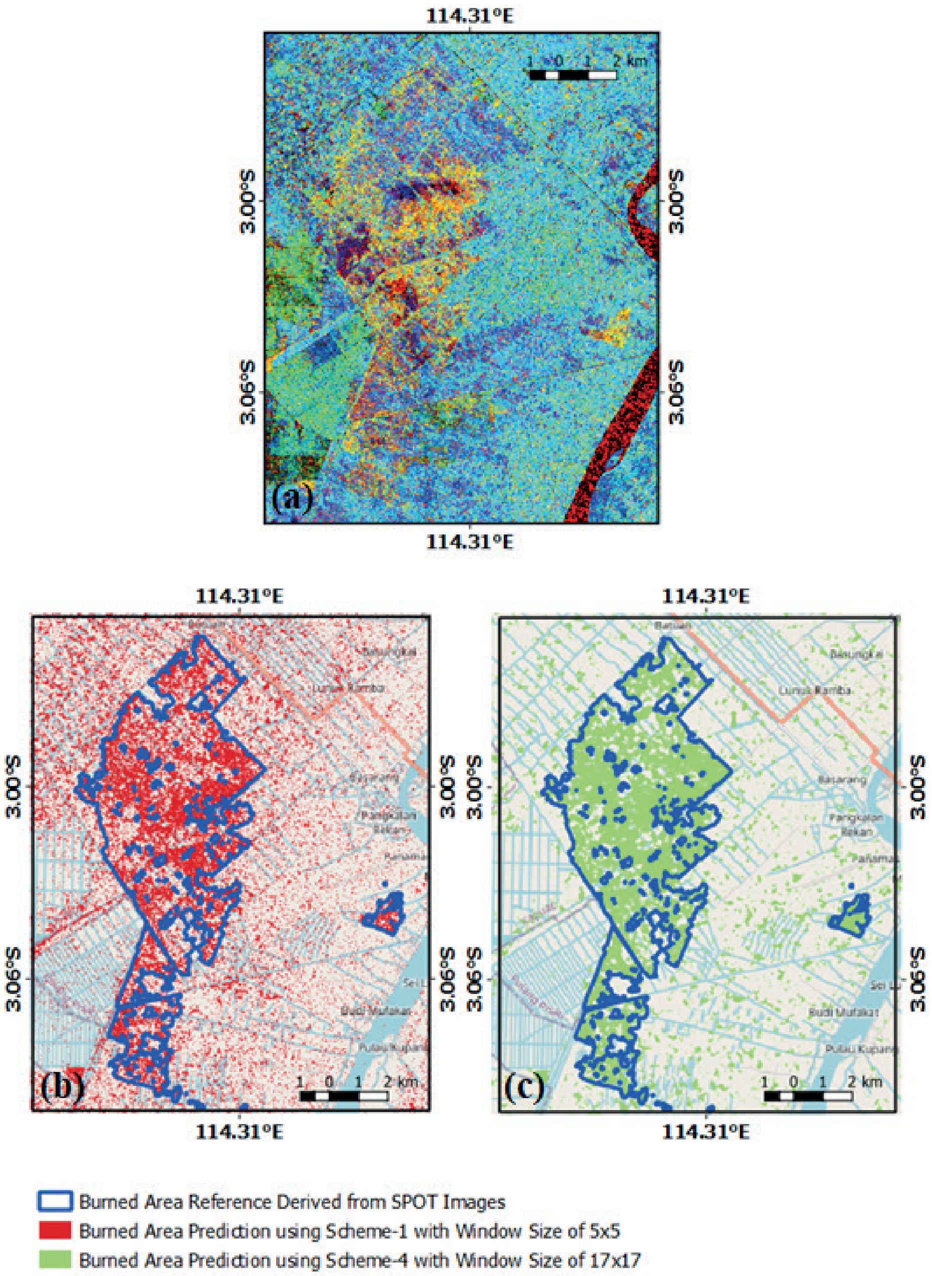

Fig. 6. (a) Sentinel-1 images of post-fire events (R= $VH_{pre\text{-}fire\ event} - VH_{post\text{-}fire\ event}$, G = $VV_{pre\text{-}fire\ event}$, B = $VH_{post\text{-}fire\ event}$); (b) The burned area detection result using scheme -1 with window size of 5×5; (c) The burned area detection result using Scheme -4 with window size of 17×17

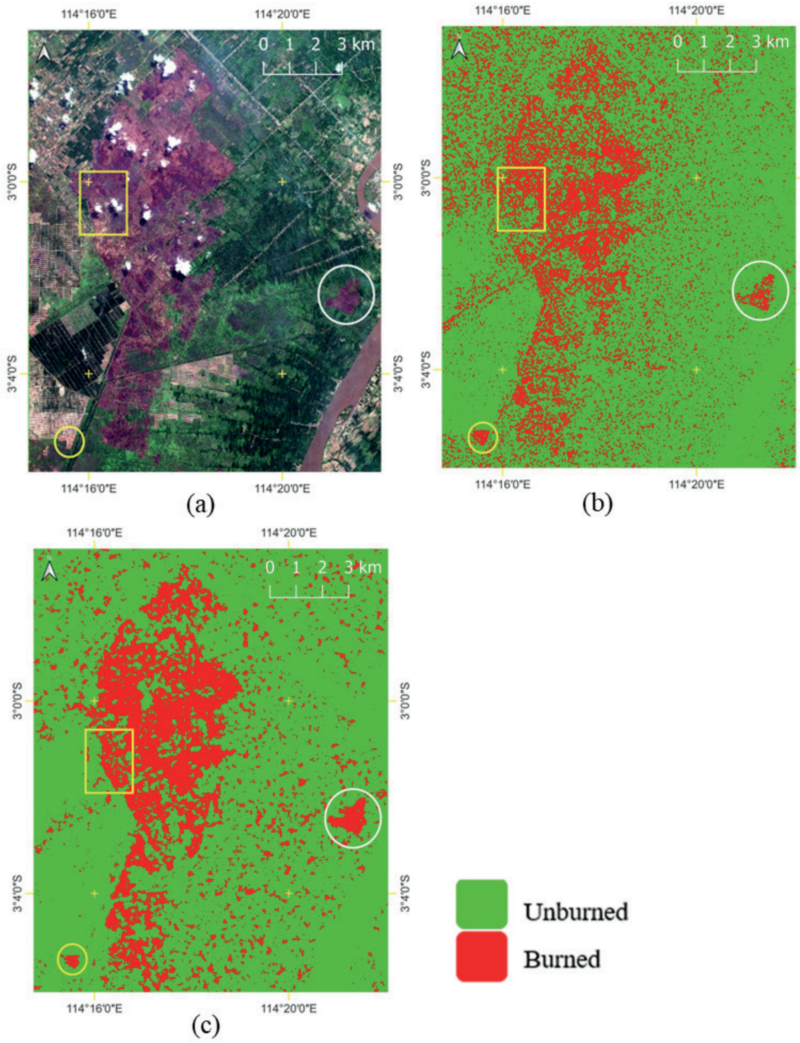

Fig. 7. A subset of burned area; (a) SPOT image as reference; (b) classification result Scheme -1 with window size of 5×5; (c) classification result Scheme -4 with window size of 17×17

The subset of burned area for the best performance scheme and SPOT images were then calculated with the WGS 1984 PDC Mercator as a reference projection system to compare both burned areas. For the model with the highest OA, precision, F1-Score, and K values which is in Scheme -4 with a window size of 17×17, the burned area prediction is up to 4,974.72 ha, whereas the burned area from SPOT images is 4,521.51 ha. It exhibits that the selected subset of burned area estimation using Scheme -4 had approximately 90% agreement with the reference data, SPOT images.

The model in Scheme -4 was also tested in the same area in a different year, 2018. Fig. 8 depicts the burned area classification result. The OA, precision, recall, F1-Score, and K values are 0.7850; 0.8775; 0.6755; 0.7633; and 0.5722 respectively. According to these performance metrics, the model has a good capability to detect the burned area.

DISCUSSION

This research demonstrates the importance of feature and texture selection to increase the model's performance classification. In comparison to the result of (Sudiana et al. 2023), optimum features and window size could increase the evaluation parameter values while using the same classification method. The increase in OA value ranged from 0.58-13.25% with the highest in Scheme -4 which uses GLCM texture features with a window size of 17×17 and without conducting Boxcar's speckle filter. This is also consistent with Gibson et. al's findings (Gibson et al. 2023) that the mean and variance texture indices of larger window sizes (both 11 and 7) are the most important variables for fire severity and fire extent models using Sentinel-1 data. It occurs as GLCM texture features apply a probability of a pixel with a certain gray-level value meeting with a neighbour pixel with a defined gray-level value (James et al. 2021).

The high accuracy of our finding in larger window sizes also depends on the size and pattern of burned areas, which are relatively large with only a few small patches of burned area. Similar to De Luca et al. (De Luca et al. 2021) the research used a large window size (11x11) because small fires were not considered (i.e. less than 0.5 km2). A smaller window size should be considered for small and scattered burned areas. The effectiveness of using a large window size also depends on the spatial resolution of the SAR image, as the finer the spatial resolution of the SAR images, the more heterogeneous the backscatter value for each land cover (Chen et al. 2004; Dorigo et al. 2012). Moreover, Boxcar's speckle filter implements an average filter which leads to increased entropy since different scattering mechanisms can be involved along with the increase in window size (Xie et al. 2018). Furthermore, Boxcar's speckle filter tends to reduce resolution as the window size increases.

According to our research, CNN-1D is feasible to implement because its method is not too complex and does not require much training time. Therefore, this method

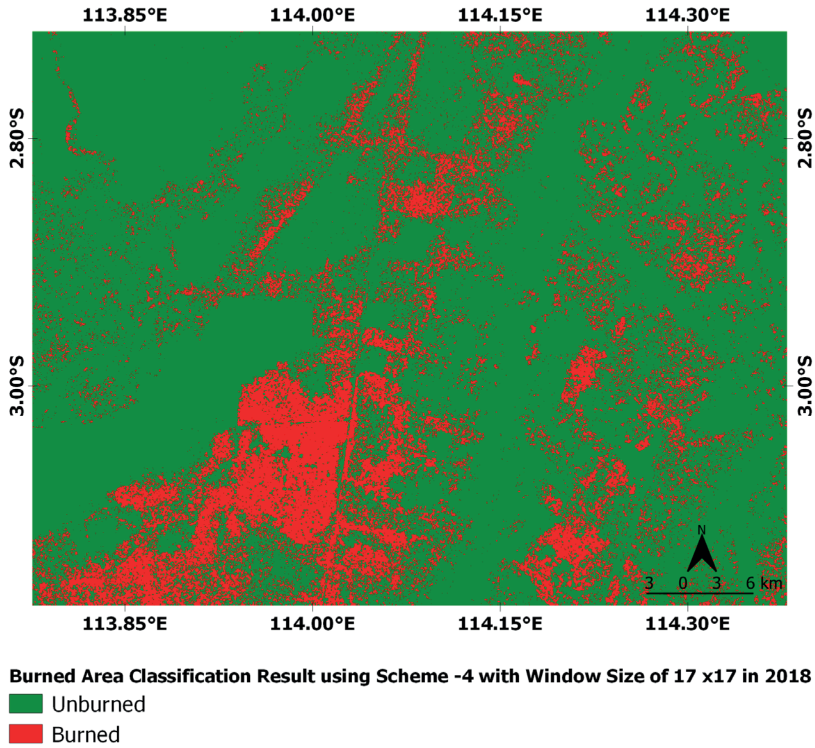

Fig. 8. Burned area classification results for 2018

is suitable for large-scale implementation. There are still numerous pixels that were misclassified since this method considers the pixel value, particularly in the agriculture area which varies seasonally and results in a change in backscatter. Therefore, the object-based approach should be considered to distinguish between the burned area and the misclassified pixels in the agriculture sector.

This research demonstrates the potential of SAR data as a complementary data for detecting burned areas, especially in situations where the observed area is cloudy, hazy, or located in a remote area. Then, by defining the optimum parameters, it may help to decrease misclassification of burned areas. In terms of time savings, window size selection does not significantly affect training time. However, the more polarimetric features and textures used, the longer the processing time.

CONCLUSIONS

This research indicated that the selection of texture features and polarimetric features is essential to optimize the performance of classification. The results obtained show that the highest overall accuracy using CNN classification was achieved at 84.61% in Scheme -4 which uses GLCM texture features and without conducting the Boxcar speckle filter on the window size of 17×17. The total burned area in the area of interest reaches 76,098.6 ha. This research shows that the burned areas in the area of interest are mainly located in shrub swamps, pure dry agriculture, and paddy fields land cover types, implying that they were caused by anthropogenic activities.

This research also shows that the performance of classification by using GLCM texture features without applying the Boxcar speckle filter is better than using intensity and polarimetric features with the Boxcar speckle filter. Furthermore, combining intensity and polarimetric features with a Boxcar speckle filter results in better classification performance than utilizing them separately. In addition, the selection of window size also helps to increase the model's performance. Compared to SPOT images as a reference, the agreement of the burned area estimation on the selected subset reaches approximately 90%.

Furthermore, based on our proposed method of using Sentinel-1 SAR data, this information can help to estimate the carbon loss of burned areas based on the fuel type (land cover) in the research area over time, even if the area is highly covered by the cloud. In future works, this model should be investigated in areas with different landscape characteristics or steep terrain areas since it is crucial. In addition, additional approaches such as decision-level-fusion need to be explored for detecting burned areas in different landscapes or steep areas.

REFERENCES

Abdikan S., Bayik C., Sekertekin A., Balcik F.B., Karimzadeh S., Matsuoka M., and Sanli F.B. (2022). Burned Area Detection Using Multi-Sensor SAR, Optical, and Thermal Data in Mediterranean Pine Forest. Forests, 13(2), 347, DOI: 10.3390/f13020347.

Anand R., Shanthi T., Sabeenian R.S., and Veni S. (2023). GLCM Feature-Based Texture Image Classification Using Machine Learning Algorithms. In: B.V. Kumar., P. Sivakumar., B. Surendiran., and J. Ding, eds., Smart Computer Vision EAI/Springer Innovations in Communication and Computing, Cham: Springer Nature, 103-125, DOI: 10.1007/978-3-031-20541-5_5.

Ansari J., Ghosh S.M., Dev Behera M., and Gupta K. S. (2020). A Study on Speckle Removal Techniques for Sentinel-1A SAR Data Over Sundarbans, Mangrove Forest, India. 2020 IEEE India Geoscience and Remote Sensing Symposium (InGARSS), 90-93, DOI: 10.1109/InGARSS48198.2020.9358929.

Arjasakusuma S., Kusuma S.S., Vetrita Y., Prasasti I., and Arief R. (2022). Monthly Burned-Area Mapping Using Multi-Sensor Integration of Sentinel-1 and Sentinel-2 and Machine Learning: Case Study of 2019's Fire Events in South Sumatra Province, Indonesia. Remote Sensing Applications: Society and Environment, 27, 100790, DOI: 10.1016/j.rsase.2022.100790.

Ban Y., Zhang P., Nascetti A., Bevington A.R., and Wulder M.A. (2020). Near Real-Time Wildfire Progression Monitoring with Sentinel-1 SAR Time Series and Deep Learning. Scientific Reports, 10(1), 1–15, DOI: 10.1038/s41598-019-56967-x.

Center for Kalimantan Ecoregion Development Control Ministry of Environment and Forestry Republic of Indonesia. (2016). Capacity of Natural Resources and The Environment of The Kalimantan Ecoregion Based on Ecosystem Services. (in Indonesian). Palangkaraya: Central Kalimantan Province Environmental Agency.

Central Kalimantan Province Environmental Agency. (2020). Environmental Performance Information Document in 2019 for Central Kalimantan Province. (in Indonesian). Palangkaraya: Central Kalimantan Province Environmental Agency.

Champion I., Germain C., Da Costa J.P., Alborini A., and Dubois-Fernandez P. (2014). Retrieval of Forest Stand Age from SAR Image Texture for Varying Distance and Orientation Values of The Gray Level Co-Occurrence Matrix. IEEE Geosci. Remote Sensing Lett., 11(1), 5–9, DOI: 10.1109/LGRS.2013.2244060.

Chen D., Stow D.A., and Gong P. (2004). Examining The Effect of Spatial Resolution and Texture Window Size on Classification Accuracy: An Urban Environment Case. International Journal of Remote Sensing, 25, 2177–2192, DOI: 10.1080/01431160310001618464.

De Luca G., Silva J.M.N., and Modica G. (2021). A Workflow Based on Sentinel-1 SAR Data and Open-Source Algorithms for Unsupervised Burned Area Detection in Mediterranean Ecosystems. GIScience & Remote Sensing, 58(4), 516-541, DOI: 10.1080/15481603.2021.1907896.

Dekker R.J. (2003). Texture Analysis and Classification of ERS SAR Images for Map Updating of Urban Areas in The Netherlands. IEEE Trans. Geosci. Remote Sensing, 41(9), 1950–1958, DOI: 10.1109/TGRS.2003.814628.

Dorigo W., Lucieer A., Podobnikar T., and Čarni A. (2012). Mapping Invasive Fallopia Japonica by Combined Spectral, Spatial, and Temporal Analysis of Digital Orthophotos. International Journal of Applied Earth Observation and Geoinformation, 19, 185–195, DOI: 10.1016/j.jag.2012.05.004.

Efransjah., Murniningtyas S., Muttaqin M.Z., eds., (2022). The state of Indonesia's Forests 2022. Jakarta: Ministry of Environtment and Forestry.

Efransjah., Murniningtyas S., Erwinsyah., and Damayanti, E.K., eds., (2020). The state of Indonesia's Forests 2020. Jakarta: Ministry of Environtment and Forestry.

Emery W.J. and Camps A. (2017). Introduction to Satellite Remote Sensing: Atmosphere, Ocean, Land and Cryosphere Applications. Amsterdam, Netherlands: Elsevier, DOI: 10.1016/C2015-0-04517-8.

Gaveau D.L.A., Descals A., Salim M.A., Sheil D., and Sloan S. (2021). Refined Burned-Area Mapping Protocol Using Sentinel-2 Data Increases Estimate of 2019 Indonesian Burning. Earth System Science Data, 13(11), 5353–5368, DOI: 10.5194/essd-13-5353-2021.

Gibson R. K., Mitchell A., and Chang H.C. (2023). Image texture analysis enhances classification of fire extent and severity using Sentinel 1 and 2 satellite imagery. Remote Sensing, 15(14), 3512, DOI: 10.3390/rs15143512.

Guidic, D. and Clark M. (2017). One-Dimensional Convolutional Neural Network Land-Cover Classification of Multi-Seasonal Hyperspectral Imagery in The San Francisco Bay Area, California. Remote Sensing, 9(6), 629, DOI: 10.3390/rs9060629.

Ho A.F.W., Zheng H., Earnest A., Cheong K.H., Pek P.P., Seok J.Y., Liu N., Kwan Y.H., Tan J.W.C., Wong T.H., Hausenloy D.J., Foo L.L., Tan B.Y.Q., and Ong M.E.H. (2019). Time-Stratified Case Crossover Study of The Association of Outdoor Ambient Air Pollution with The Risk of Acute Myocardial Infarction in The Context of Seasonal Exposure to The Southeast Asian Haze Problem. Journal of the American Heart Association, 8(6), e011272, DOI: 10.1161/JAHA.118.011272.

Hossain A.K.M.A. and Easson G. (2009). Microwave remote sensing of soil moisture in semi-arid environment. InTech, DOI: 10.5772/8301.

Hosseini M. and Lim S. (2023). Burned Area Detection Using Sentinel-1 SAR Data: A Case Study of Kangaroo Island, South Australia. Applied Geography, 151, 102854, DOI: 10.1016/j.apgeog.2022.102854.

Ismail A.S., Gao X., and Deng C. (2014). SAR Image Classification Based on Texture Feature Fusion. 2014 IEEE China Summit & International Conference on Signal and Information Processing (ChinaSIP), 153-156, DOI: 10.1109/ChinaSIP.2014.6889221.

James J., Heddallikar A., Choudhari P., and Chopde S. (2021). Analysis of Features in SAR Imagery Using GLCM Segmentation Algorithm. In: G.K.Verma, B. Soni, S. Bourennane, and A.C.B. Ramos, eds., Transactions on Computer Systems and Networks Data Science: Theory, Algorithms, And Applications. Singapore: Springer Singapore, 253-266, DOI: 10.1007/978-981-16-1681-5.

Kiranyaz S., Avci O., Abdeljaber O., Ince T., Gabbouj M., and Inman D.J. (2021). 1D Convolutional Neural Networks and Applications: A Survey. Mechanical Systems and Signal Processing, 151, 107398, DOI: 10.1016/j.ymssp.2020.107398.

Landis J.R. and Koch G.G. (1977). The Measurement of Observer Agreement for Categorical Data. Biometrics, 33(1), 159-174.

Lasaponara R. and Tucci B. (2019). Identification of Burned Areas and Severity Using SAR Sentinel-1. IEEE Geosci. Remote Sensing Lett., 16(6), 917–921, DOI: 10.1109/LGRS.2018.2888641.

LeCun Y., Bengio Y., and Hinton G. (2015). Deep Learning. Nature, 521(7553), 436–444, DOI: 10.1038/nature14539.

Lestari A.I., Rizkinia M., and Sudiana D. (2021). Evaluation of Combining Optical and SAR Imagery for Burned Area Mapping Using Machine Learning. 2021 IEEE 11th Annual Computing and Communication Workshop and Conference (CCWC), 52-59, DOI: 10.1109/CCWC51732.2021.9376117.

Luft H., Schillaci C., Ceccherini G., Vieira D., and Lipani A. (2022). Deep Learning Based Burnt Area Mapping Using Sentinel 1 for The Santa Cruz Mountains Lightning Complex (CZU) and Creek Fires 2020. Fire, 5(5), 163, DOI: 10.3390/fire5050163.

Mandal D., Kumar V., Ratha D., Dey S., Bhattacharya A., Lopez-Sanchez J.M., McNairn H., and Rao Y.S. (2020). Dual Polarimetric Radar Vegetation Index for Crop Growth Monitoring Using Sentinel-1 SAR Data. Remote Sensing of Environment, 247,111954, DOI: 10.1016/j.rse.2020.111954.

Ministry of Environment and Forestry (MoEF) Republic of Indonesia. (2019). Recapitulation of Forest and Land Fire Area (Ha) per Province in Indonesia. (in Indonesian). [online] Available at: https://sipongi.menlhk.go.id/ [Accessed 21 Apr 2023].

Molin S. and Jee K. (2021). Hands-On Data Analysis with Pandas: A Python Data Science Handbook for Data Collection, Wrangling, Analysis, and Visualization. Birmingham: Packt Publishing.

Mullissa A.G., Marcos D., Tuia D., Herold M., and Reiche J. (2022). deSpeckNet: Generalizing Deep Learning-Based SAR Image Despeckling. IEEE Trans. Geosci. Remote Sensing, 60, 1–15, DOI: 10.1109/TGRS.2020.3042694.

Murashkin D., Spreen G., Huntemann M., and Dierking W. (2018). Method for Detection of Leads from Sentinel-1 SAR Images. Ann. Glaciol., 59,124–136, DOI: 10.1017/aog.2018.6.

Mutai, S.C. (2019). Analysis of Burnt Scar Using Optical and Radar Satellite Data. Master thesis. Enschede: University of Twente.

Nguyen L.S.P., Chang J.H.W., Griffith S.M., Hien T.T., Kong S.S.K., Le H.N., Huang, H.Y., Sheu, G.R., and Lin, N.H. (2022). Trans-Boundary Air Pollution in A Southeast Asian Megacity: Case Studies of The Synoptic Meteorological Mechanisms and Impacts on Air Quality. Atmospheric Pollution Research, 13, 101366, DOI: 10.1016/j.apr.2022.101366.

Periasamy, S. (2018). Significance of Dual Polarimetric Synthetic Aperture Radar in Biomass Retrieval: An Attempt on Sentinel-1. Remote Sensing of Environment, 217, 537–549, DOI: https://doi.org/10.1016/j.rse.2018.09.003.

Radman A., Shah-Hosseini R., and Homayouni S. (2023). An Unsupervised Saliency-Guided Deep Convolutional Neural Network for Accurate Burn Mapping from Sentinel-1 SAR Data. Remote Sensing, 15(5), 1184, DOI: 10.3390/rs15051184.

Sakti A.D., Anggraini T.S., Ihsan K.T.N., Misra P., Trang N.T.Q., Pradhan B., Wenten I.G., Hadi P.O., and Wikantika K. (2023). Multi-Air Pollution Risk Assessment in Southeast Asia Region Using Integrated Remote Sensing and Socio-Economic Data Products. Science of The Total Environment. 854, 158825, DOI: 10.1016/j.scitotenv.2022.158825.

Singh M. and Kaur G. (2011). SAR Image Classification Using PCA and Texture Analysis. In: Das, V.V., Thomas, G., Lumban Gaol, F., eds., Information Technology and Mobile Communication, Communications in Computer and Information Science. Heidelberg: Springer Berlin., 435-439, DOI: 10.1007/978-3-642-20573-6_78.

Small D. (2011). Flattening Gamma: Radiometric Terrain Correction for SAR Imagery. IEEE Trans. Geosci. Remote Sensing, 49(8), 3081–3093, DOI: 10.1109/TGRS.2011.2120616.

Soh L.K. and Tsatsoulis C. (1999). Texture Analysis of SAR Sea Ice Imagery Using Gray Level Co-Occurrence Matrices. IEEE Trans. Geosci. Remote Sensing, 37(2),780–795.

Song Y., Zhang Z., Baghbaderani R.K., Wang F., Qu Y., Stuttsy, C., and Qi H. (2019). Land Cover Classification for Satellite Images Through 1D CNN, 10th Workshop on Hyperspectral Imaging and Signal Processing: Evolution in Remote Sensing (WHISPERS), 1-5, DOI: 10.1109/WHISPERS.2019.8921180.

Gupta D. K., Prashar S., Singh S., Srivastava, P.K., and Prasad, R. (2022). Introduction to Radar Remote Sensing. In: P.K. Srivastava, D.K. Gupta, T. Islam, D. Han, and R. Prasad, eds., Radar Remote Sensing: Applications and Challenges, Earth Observation Series. Amsterdam: Elsevier, 3-27, DOI: 10.1016/B978-0-12-823457-0.00018-5

Statistics Indonesia. (2010). Kapuas in Figures 2010. Kuala Kapuas, Kapuas: Statistic of Kapuas Regency.

Statistics Indonesia. (2023). Pulang Pisau Regency in Figures 2023. Kahayan Hilir, Pulang Pisau: Statistics of Pulang Pisau Regency.

Sudiana D., Lestari A.I., Riyanto I., Rizkinia M., Arief R., Prabuwono A.S., and Sumantyo J.T.S. (2023) A Hybrid Convolutional Neural Network and Random Forest for Burned Area Identification with Optical and Synthetic Aperture Radar (SAR) Data. Remote Sensing, 15(3), 728, DOI: 10.3390/rs15030728.

Tanase M.A., Belenguer-Plomer M.A., Roteta E., Bastarrika A., Wheeler J., Fernández-Carrillo Á., Tansey K., Wiedemann W., Navratil P., Lohberger S., Siegert F., and Chuvieco E. (2020). Burned Area Detection and Mapping: Intercomparison of Sentinel-1 and Sentinel-2 Based Algorithms Over Tropical Africa. Remote Sensing, 12(2), 334, DOI: 10.3390/rs12020334.

Tanase M.A., Santoro M., Riva J.D.L., Pérez-Cabello F., and Toan T.L. (2010). Sensitivity of X-, C-, And L-Band SAR Backscatter to Burn Severity in Mediterranean Pine Forests. IEEE Transactions on Geoscience and Remote Sensing, 48(10), 3663-3675, DOI: 10.1109/TGRS.2010.2049653.

Wen C., ZhangY., and Deng K. (2009). Urban Area Classification in High Resolution SAR Based on Texture Features. The International Conference on Geo-spatial Solutions for Emergency Management and the 50th Anniversary of the Chinese Academy of Surveying and Mapping, Beijing, China, 281-285.

Xie J., Li Z., Zhou C., Fang Y., and Zhang Q. (2018). Speckle Filtering of GF-3 Polarimetric SAR Data with Joint Restriction Principle. Sensors, 18(5), 1533, DOI: 10.3390/s18051533.

Yahia M., Ali T., Mortula M.M., Abdelfattah R., Mahdy S.E., and Arampola N.S. (2020). Enhancement of SAR Speckle Denoising Using The Improved Iterative Filter. IEEE J. Sel. Top. Appl. Earth Observations Remote Sensing, 13, 859–871, DOI: 10.1109/JSTARS.2020.2973920.

Yeung J. (2019) Indonesian forests are burning, and Malaysia and Singapore are choking on the fumes. [online] Available at: https://www.huahintoday.com/sports/indonesian-forests-still-burning-and-malaysia-and-singapore-are-choking-on-the-fumes/#:~:text=More%20than%20930%2C000%20hectares%20%28about%202.3%20million%20acres%29,all%20week%2C%20with%20air%20quality%20reaching%20unhealthy%20levels [Accessed 20 June 2023].

Zhang C., PanX., Li H., Gardiner A., Sargent I., Hare J., and Atkinson P.M. (2018). A Hybrid MLP-CNN Classifier for Very Fine Resolution Remotely Sensed Image Classification. ISPRS Journal of Photogrammetry and Remote Sensing, 140,133–144, DOI: 10.1016/j.isprsjprs.2017.07.014.